15TH IEA HEAT PUMP CONFERENCE
MAY 26–29, 2026 | HOFBURG
VIENNA 2026
DECARBONISATION THROUGH INNOVATION

A comprehensive methodology for optimal High-Temperature Heat Pump design: integrating working fluid, cycle configuration, and component selection across a wide high-temperature operating range

M A. Hamada[a,*], Manuele Gatti[a], Luca Molinaroli[a]

[a]Politecnico di Milano, Department of Energy, via Lambruschini 4, Milan 20156, Italy

Abstract

High-Temperature Heat Pump offer transformative solutions for most industrial application, potentially reducing CO_2 emissions by 148 Mt/a. However, their implementation faces challenges and competition from traditional energy systems, requiring strategic enhancements in design. The primary obstacle lies in absence of standardized methodologies for the optimal system design for each industrial application, as each case requires a specific model that is difficult to adapt to different operating conditions. Many studies examined cycle configuration and working fluid selection, but they often investigated these aspects independently and relied on fixed literature correlations to predict component performance. Hence, a detailed numerical model was developed and validated to simulate 59 potential refrigerants across six different cycle configurations, using five different compressors and two heat exchanger technologies. For each possible combination, energetic-economic-environmental analysis (including levelized cost of heat considering carbon tax) was evaluated across wide range of operating conditions (source temperature: 0:100 °C, sink temperature: 100:200 °C). The finding showed that single-stage cycles were optimal at temperature lifts <80 K, while cascade cycles dominated at higher lifts, and two-stage flash cycles were optimal in selected intermediate cases. Cyclopentane, n-pentane, and methoxymethane delivered the best performance, either alone in single-stage cycles or paired in cascade systems. Multi-stage centrifugal compressors were optimal across most conditions. Optimal designs converged to a Carnot efficiency of ~0.6. Compressor costs dominated the specific equipment cost (~60–70%), with heat exchangers contributing ~30%. Electricity consumption was the main levelized cost of heat driver (~60%), followed by CO_2-emission taxes (~15%) and capital cost (~20%).

Keywords: High-Temperature Heat Pump; Cycle configuration; Refrigerant; Carnot efficincy; Specific equipement cost; Levelized cost of heat

1. Introduction

Process heating accounts for a significant portion of European industrial energy demand, with 37% required below 200 °C. Deploying High-Temperature Heat Pumps (HTHPs) in this sector could reduce CO_2 emissions by up to 148 Mt/a [1]. While HTHPs are commercially mature for small-scale processes and temperatures below 120–130 °C, large-scale applications with high temperature lifts (ΔT_{lift}) remain challenging due to technological and methodological challenges. The primary challenge is the lack of a standardized approach for optimizing HTHPs for each industrial process, as each case requires a specific model, which is often time-intensive to adapt to specific situations and working conditions. Previous studies have investigated cycle configuration or working fluid selection, but typically these aspects have been independently examined. Furthermore, these studies often relied on fixed or simplified correlations to predict critical components (compressor, heat exchanger (HEX)) performance. Optimizing HTHP performance necessitates tailoring the cycle and working fluid to specific application requirements. However, few studies simultaneously evaluate cycle configuration and working fluid selection across broad temperature ranges, and existing studies [2-4]

* Corresponding author. Tel.: +39 351 301 7076
E-mail address: mohamedali.hamada@polimi.it

15th IEA Heat Pump Conference 2026 - HTH2.1 - https://doi.org/10.23697/1mky-6960

outline one-stage, two-stage, and cascade cycles but did not determine which configurations deliver the optimal performance under specific operating conditions. Consequently, the literature lacks a comprehensive and detailed numerical framework for identifying the optimal HTHP design. This study addresses this gap by developing a validated numerical model to optimize the HTHP design, including cycle configuration, fluid, and compressors and HEXs technologies selection. Then, the model evaluates performance across a broad range of high-temperature conditions using key performance indicators (KPIs) that integrate thermodynamic, economic, and environmental criteria, aiming to identify optimal designs for industrial applications up to 200 °C and reduce uncertainty in system selection.

2. Methodology

This study employed numerical models developed in MATLAB™ v2023a, with REFPROP 10.0 [5] for thermophysical properties, to identify optimal HTHP designs. This study started with the analysis of key input parameters, which served as the decision variables: heat source temperature, heat sink temperature, and heating capacity. The heat sink outlet temperature ($T_{sink,out}$) and heat source outlet temperature ($T_{source,out}$) were varied between 100–200 °C and 0–100 °C, respectively, with ΔT_{lift} ranging from 20-180 K. The heat source temperature glide (ΔT_{source}) was fixed at 10 K, with a condenser heating capacity of 5 MW of steam at $T_{sink,out}$. Inlet sink temperature is subcooled water by 3 °C (it exited the condenser as saturated steam at $T_{sink,out}$). The model evaluated 59 working fluids within six advanced HTHP cycle configurations, with five compressors and two HEXs to compare how all possible combinations of all these aspects could influence overall efficiency. The methodology started with a pre-screening of working fluids, followed by their classification according to the required supply temperature to further reduce the candidate set. Subsequently, appropriate compressor and HEX technologies were selected based on the target heating capacity. Finally, the system layout was optimized to achieve optimal energetic, economic, and environmental performance. The configurations were specifically chosen to highlight the potential of various cycles under these conditions. These included cycles with an Internal Heat Exchanger (IHX) to ensure dry compression and improve performance, two-stage compression cycles to decrease high compressor discharge temperature, and cascade cycles, which connected two basic cycles, offered flexibility of using different refrigerants in each loop, making them suitable for high ΔT_{lift} processes. The schematics and pressure-enthalpy (P-h) diagrams for all configurations were detailed in Fig. 1.

This research introduced a three-step framework that evaluated the interplay between cycle configuration, working fluid, compressors, and HEX technologies. The process involved: (1) pre-screening candidate working fluids; (2) assessing thermodynamic, economic, and environmental performance of each possible HTHP design; and (3) comparing the top-performing designs to identify the optimal solution.

2.1. Working fluids pre-screening

Refrigerant selection is a critical factor in HTHP design, influencing cycle design, compressor discharge temperatures, energetic efficiency, and component selection. Due to increasingly stringent environmental regulations, fluids with zero ozone depletion potential (ODP) and low global warming potential (GWP) are indispensable. Additionally, thermodynamic properties must be compatible with specific working conditions.

The screening of applicable refrigerants was therefore based on a multi-stage pre-screening process. From an initial pool of 59 refrigerants, a primary filter was applied based on environmental criteria (GWP, ODP), which yielded 29 candidates (R-1233zd(E), R-1224yd(Z), R-1234ze(Z), R-1336mzz(Z), R-1234yf, R-1234ze(E), R-1216, R-1243zf, R-1336mzz(E), methoxymethane, ammonia, water, CO_2, cyclopropane, cyclopentane, propane, propene, n-pentane, isobutane, isopentane, butane, acetylene, ethane, ethylene, R-161, R-1123, R-41, R-123, R-152a). These 29 fluids were then validated for their thermophysical properties (e.g., critical temperature, Normal Boiling Point) to ensure their applicability across the target operating conditions).

2.2. Energetic, economic, and environmental performance of all possible combinations

This section outlined the methodology to calculate the KPIs to compare possible combinations of working fluids, cycle configurations, and compressor and HEX technologies across all the temperature conditions. A standard set of design parameters and general assumptions was applied to all simulations. Thermal and pressure losses were neglected, and expansion valves were assumed isenthalpic. A minimum pinch temperature difference of 2 °C was imposed, with 5 °C superheating at evaporator outlet and 3 °C subcooling at condenser exit. IHX effectiveness was set at 0.75. In two-stage compression systems, intermediate pressure was defined as the geometric mean of evaporation and condensation pressures. For cycles including flash tank, ideal vapor–

liquid separation was assumed. Vapor leaving economizers was superheated by 5 °C, and mass fraction was iteratively adjusted to satisfy second law of thermodynamics. For trans-critical cycles, gas cooler pressure was optimized iteratively, starting at 10% above the critical pressure, to meet the minimum pinch temperature requirement (0.5 °C). models were based on steady-state energy and mass balance equations.

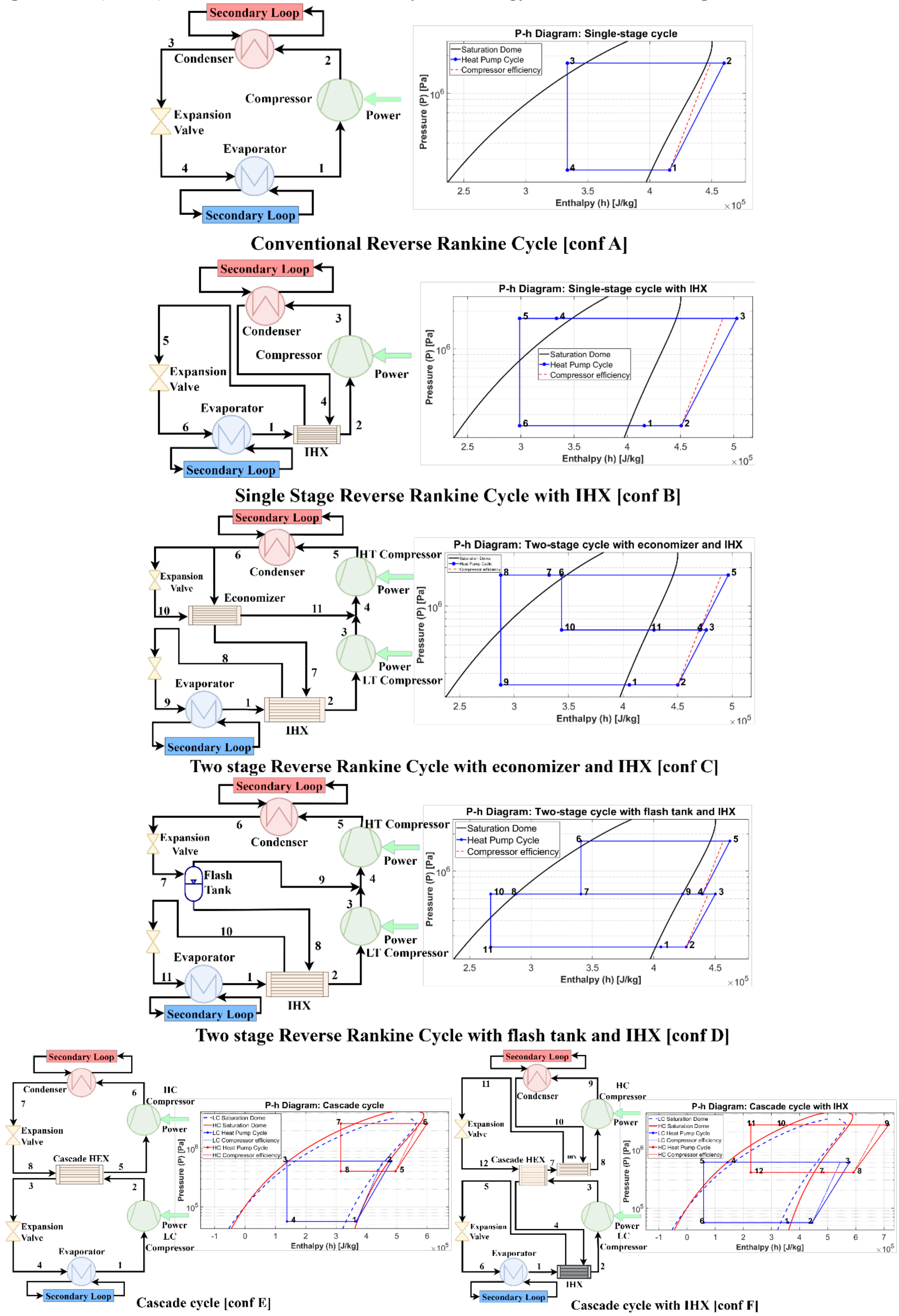

Figure 1: The schematics and pressure-enthalpy (P-h) diagrams for all configurations

The key metrics, which used in the final step to identify the optimal system, included energetic performance (COP, Carnot efficiency, η_{carnot}), economic feasibility (specific purchase equipment cost, SPEC), environmental impact (Total Equivalent Warming Impact, TEWI), and the main objective (Levelized Cost of Heat when considering carbon tax, $LCOH_{GCT}$) were computed using four interconnected models.

2.2.1. Thermodynamic model

The model first evaluated refrigerant properties at all cycle state points. After determining these states, the COP was computed (Eq. 1) as the ratio between heating capacity (Q_{sink}) and required compressor electric power (P_{comp}), where the latter was obtained using the compressor efficiencies. While constant compressor efficiencies were often assumed, the wide range of suction and discharge temperatures leaded to significant variations in pressure and volume ratios; influencing the efficiency. Therefore, a more detailed efficiency model was adopted in the sizing model. Although COP is the standard performance metric for heat pumps, it becomes unsuitable when comparing systems across different ΔT_{lift}. In such cases, η_{carnot} (Eq. 2) provided a more meaningful indicator, as it related performance to the thermodynamic limit.

$$COP = Q_{sink}/P_{comp} \tag{1}$$

$$\eta_{carnot} = COP/COP_{carnot}\ ,\ COP_{carnot} = T_{sink}/\Delta T_{lift} \tag{2}$$

2.2.2. Sizing model

Accurate sizing of key components (compressors and HEXs) is essential for reliable energetic, economic, and environmental assessment. Because HEX size and compressor load and size could vary with operating conditions, detailed sizing models were required. The following sections described the approaches adopted.

2.2.2.1. Compressor Model

Compressors are the main power-consuming components and strongly influence system performance. As different applications may require different technologies, five compressors (reciprocating, screw, low-speed turbo, centrifugal, and turbo-fan) were assessed, including multi-unit for large volumetric flow rates and multi-stage for high pressure ratios. For each type, appropriate ranges of flow rate and pressure ratio were defined. To model performance, type-specific efficiencies (i.e., isentropic and volumetric or polytropic) were estimated as functions of pressure ratio at average flow rate, based on manufacturer data [6-9], experimental results, or validated literature models [10-20]. A constant electromechanical efficiency ($\eta_{el,mec}$) of 0.95 was assumed.

2.2.2.2. HEX Model

Modeling energy exchange and predicting flow behavior between the refrigerant and secondary fluid in the evaporator and condenser are challenging due to the presence of multiple flow regimes, hence specific correlations for each HEX were employed. The heat source fluid was assumed to be water or a water–glycol mixture, while steam was used as the secondary fluid at the heat sink. The HEX type (plate or shell-and-tube) was selected based on the required heat transfer rate, and its size was determined from convective heat transfer coefficients derived using literature correlations. For plate HEXs, the correlations by Longo et al. [21, 22] were applied to the evaporator and condenser, respectively. For shell-and-tube HEXs, the correlations by Zhang et al. [23] and Dalkilic et al. [24] were employed for the evaporator and condenser, respectively.

2.2.3. Economic Model

The economic analysis was based on estimating the SPEC using established cost correlations and the heating capacity. Total capital expenditure (CAPEX) was then calculated by applying an average escalation factor from literature [25] to the total equipment cost. This factor accounts for all associated project costs, including integration, Balance of Plant (BOP), planning, and installation. A key advantage of this method was that all cost correlations were expressed as functions of component size or capacity, allowing the economic performance to be evaluated across different system scales. Since the computed equipment costs originated from different years, they were updated to reflect current economic conditions. The Chemical Engineering Plant Cost Index (CEPCI) was utilized to adjust for inflation and variations in the time value of money. The cost correlations used for each component were presented below.

2.2.3.1. Compressor cost

The compressor cost (C_{comp}) was estimated according to the compressor type. For screw compressors, the cost primarily depended on the suction volumetric flow rate ($\dot{v}_{in}$). The correlation proposed by Ommen et al. [26], which incorporated an exponential scaling factor, was applied as shown in Eq. 3.

$$C_{comp,screw} = 19{,}850 * \left(\frac{\dot{v}_{in}}{279.8}\right)^{0.73} * CEPCI \tag{3}$$

For reciprocating compressors, the cost is mainly a function of P_{comp}. The correlation proposed by Shamoushaki et al. [27] was used, as shown in Eq. 4.

$$C_{comp,rec} = [Log(P_{comp}) + 0.04147(P_{comp})^2 + 454.8(P_{comp}) + 1.81 * 10^5] * CEPCI \tag{4}$$

For centrifugal and turbo fan compressors, another correlation developed by Shamoushaki et al. [27] was utilized, as displayed in Eq. 5.

$$C_{comp,cen} = [Log(P_{comp}) + 0.03867(P_{comp})^2 + 446.7(P_{comp}) + 1.378 * 10^5] * CEPCI \tag{5}$$

2.2.3.2. HEXs cost

The cost of HEXs was calculated based on their type and heat transfer area ($A_{HEX,i}$). For shell-and-tube HEXs, the formula from Hosseinnia et al. [28] was applied (Eq. 6), using the correction factors (f_M, f_P, f_T) detailed in Table 1. For plate-type HEXs, the cost was given by Eq. 7, as developed by Ommen et al. [26].

$$C_{HEX,S\&T} = 32{,}800\left(\frac{A_{HEX,i}}{80}\right)^{0.68} f_M * f_P * f_T * CEPCI \tag{6}$$

$$C_{HEX,p} = 15{,}526 * \left(\frac{A_{HEX,i}}{42}\right)^{0.8} * CEPCI \tag{7}$$

Table 1: Shell and tube HEXs factors [28]

Parameter		f_M	f_P	f_T
Shell and tube HEX	Condenser	2.40	1.06	1.30
	Evaporator	2.40	1.00	1.00
	Cascade HEX	1.70	1.04	1.03

2.2.3.3. Flash tank (FT) cost

The cost of FT was estimated using the correlation by Mosaffa et al. [29], which was based on the mass flow rate $\dot{m}$, as shown in Eq. 8.

$$C_{FT} = 280.3 * \dot{m}_{ref}^{0.67} * CEPCI \tag{8}$$

2.2.3.4. Throttling valve (TV) cost

The cost of TV was calculated by another correlation proposed by Mosaffa et al. [29], which was based on the mass flow rate $\dot{m}$, as shown in Eq. 9.

$$C_{TV} = 114.5 * \dot{m}_{ref} * CEPCI \tag{9}$$

An exchange rate from USD to € was applied for the reciprocating and centrifugal compressors, shell-and-tube HEXs, FTs, and TVs as their cost correlations were originally expressed in USD. The total equipment cost is obtained by summing all component costs. SPEC, expressed in €/kW$_{TH}$, was then calculated by dividing this total by the condenser-side heating capacity. The total equipment cost represented the manufacturer's purchase cost for all components. Additional expenses, such as integration, balance of plant (BOP), planning, and installation, were incorporated to evaluate the total CAPEX by applying an escalation factor (f_{ins}).

2.2.3.5. Operation expenses (OPEX)

OPEX consisted of the electricity cost for operating the heat pump (*OPC*) and a fixed annual operation and maintenance cost (*O&MC*). The *O&MC* was set to 4% of the compressors and HEXs cost and 2% for all other components. *OPC* was calculated from P_{comp}, the annual operating hours (h_{op}), and the specific electricity purchase price (Cs_{elec}), which excluded any carbon-tax component from the grid mix.

Total annual cost (*TAC*), expressed in €/y, was evaluated from the total CAPEX, OPEX (O&M and OPC), and the capital charge factor (CF), as defined in Eq. 10. All related parameters were summarized in Table 2.

$$TAC = \sum_{i=1}^{n} f_{ins} * CF * C_i + O\&MC_i + OPC \tag{10}$$

Table 2: parameters of the economic model

Parameter	Value	Ref.
Specific electricity purchase price (Cs_{elec}), excluding carbon tax associated to CO_2 emissions from electricity mix	100 €/MWh	[30]
Annual interest rate (i)	8%	
Lifetime (n)	20 years	
Annual full-load operating hours (h_{op})	8,000 hours/y	
Exchange rate from USD to €	0.9	
Cost escalation factor for integration, Balance of Plant (BOP), planning, and installation (f_{ins})	2.5	[25]

2.2.4. Environmental Model

TEWI was evaluated [31, 32] (Eq. 11) to assess the carbon footprint of the analyzed systems. This metric combined the direct impact, which was governed by the refrigerant's GWP and was independent of input p_{comp} and operating conditions, with the indirect impact, which was primarily driven by electric energy consumption. The latter typically being dominant unless a fully renewable power mix was used, all related parameters were detailed in Table 3.

$$TEWI = GWP * L_a * n + GWP * m_{ch} * (1 - \alpha) + n * P_{comp} * h_{op} * \beta \tag{11}$$

Table 3: parameters used in TEWI evaluation

Parameter	Value	Ref.
Charging mass (m_{ch})	100 kg / MW of heating capacity	
The annual refrigerant leakage (L_a)	5% of m_{ch}	[32]
The recycling factor of the refrigerant (α)	85%	
Fossil CO_2 emissions from electricity consumption (β)	0.2958 kg/kWh	[32]

2.3. Screening of the optimal combination

A post-processing model identified the optimal system configuration, working fluid, and component technology by jointly considering energetic, economic, and environmental metrics, with $LCOH_{GCT}$ as the primary objective. As shown in Eq. 13, $LCOH_{GCT}$ accounted for the Carbon Tax (CT). Based on yearly EU Carbon Permits, CT of 80 €/tCO_2 was utilized [33]. The tax is applied to both Scope 1 (refrigerant leakage, direct) and Scope 2 (electricity, indirect) emissions.

$$TAC_{GCT} = TAC + CT_{HP},\ CT_{HP} = CT * \frac{TEWI}{n} \tag{12}$$

$$LCOH_{GCT} = \frac{TAC_{GCT}}{Q_{sink} * h_{op}} \tag{13}$$

3. Results and discussion

This study evaluated HTHP systems, each defined by a unique combination of cycle configuration, working fluid, compressor, and HEX technology over a comprehensive operational matrix to cover most industrial process heat conditions. $T_{\text{source,out}}$ was varied from 0 °C to 100 °C (20 °C increments), representing common industrial excess heat. A 10 K glide was assumed for the heat source, reflecting typical process cooling applications (e.g., fermentation, boiling recovery). ΔT_{lift} was spanned from 20 K to 180 K (20 K increments), resulting in T_{sink} up to 200 °C. The heat sink was modelled for steam production, characteristic of high-demand industrial sectors (e.g., food and beverage, chemical distillation, paper making, pharmaceutical process, or milk dairy process).

3.1. Optimal cycle configuration and working fluid combination

While more advanced configurations with additional components yielded higher energetic performance, but energetic performance alone was insufficient. Hence, this analysis did not rely on energetic metrics alone, and also considered economic and environmental criteria, with the main objective of minimizing $\mathrm{LCOH_{GCT}}$. All feasible combinations of system configurations, working fluids, and compressor technologies were compared to identify the optimal solution at each temperature condition based on energetic, economic, and environmental KPIs as depicted in Fig. 2. The results showed a clear dependency on ΔT_{lift}. At low lifts (< 80 K), single-stage cycle configurations consistently provided the optimal solution. However, as ΔT_{lift} increased, these configurations were quickly outperformed. At high lifts (> 80 K), the cascade cycle was the optimal solution for most scenarios, followed by the two-stage cycle with a flash tank. These trends were consistent with thermodynamic expectations and served to illustrate the robustness of the proposed methodology. An application of the methodology to a brewery process is presented in Hamada et al. [34]. Regarding working fluids, cyclopentane, n-pentane, and methoxymethane were the most promising candidates, either individually in single-stage cycles or in combination within Cascade systems. Among compressor technologies, multi-stage centrifugal compressors were the optimal choice in most scenarios. This was a direct consequence of the 5 MW heating capacity, which resulted in very high volumetric flow rates. These flow rates often exceed the operational range of other compressor types. While multi-unit setups of other types could handle the flow rate, their efficiencies diminished significantly at the high-pressure ratios required. Therefore, the dominance of centrifugal compressors was highly dependent on the heating capacity; a different capacity could result in a different optimal technology. Cases highlighted in red circles indicated compressor discharge temperatures exceeding 200 °C. This surpassed the 175 °C limit of most current commercial compressors, a restriction typically imposed by refrigerant thermal stability [32]. For this analysis, a higher limit of 250 °C was adopted. This was done to reduce computational cost and to anticipate rapid technological advancements in compressor design that may soon overcome current thermal limitations.

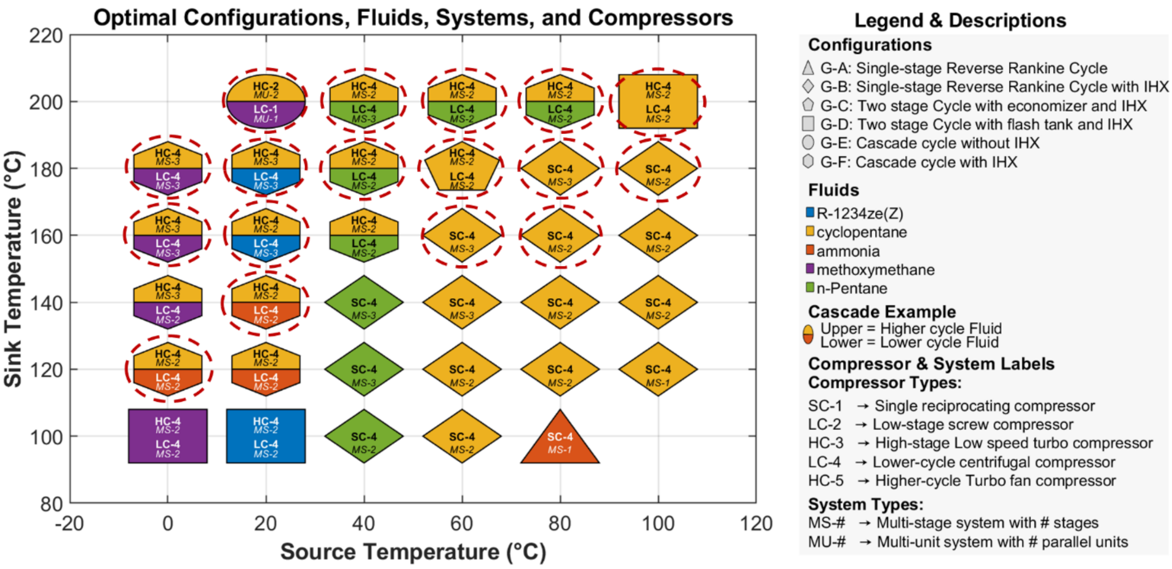

Figure 2: Optimal configuration, refrigerant, and compressor technology at each temperature condition

3.2. Energetic performance

Fig. 3 presented the COP of the optimal solution at each temperature condition, with energy performance compared using the COP and η_{carnot} parameters. The system COP depended on the system's internal energy, influenced by compressor efficiency, operating pressures, and temperatures. The results demonstrated that at a constant T_{sink}, COP decreased exponentially with increasing ΔT_{lift}. This decline was due to the rising pressure ratio associated with higher ΔT_{lift}, which also significantly reduced compressor efficiency. Across the evaluated temperature conditions, the optimal systems demonstrated a η_{carnot} consistently near 0.6. This convergence confirmed the high energetic efficiency of these solutions. For each T_{sink}, the highest η_{carnot} were observed at high ΔT_{lift} combined with low T_{source}, a condition that minimized evaporator losses, except for the optimal system at the T_{source} = 20 °C and T_{sink} = 200 °C. In contrast, the lowest η_{carnot} resulted from low ΔT_{lift} and high T_{source}, which substantially increased losses from the evaporator.

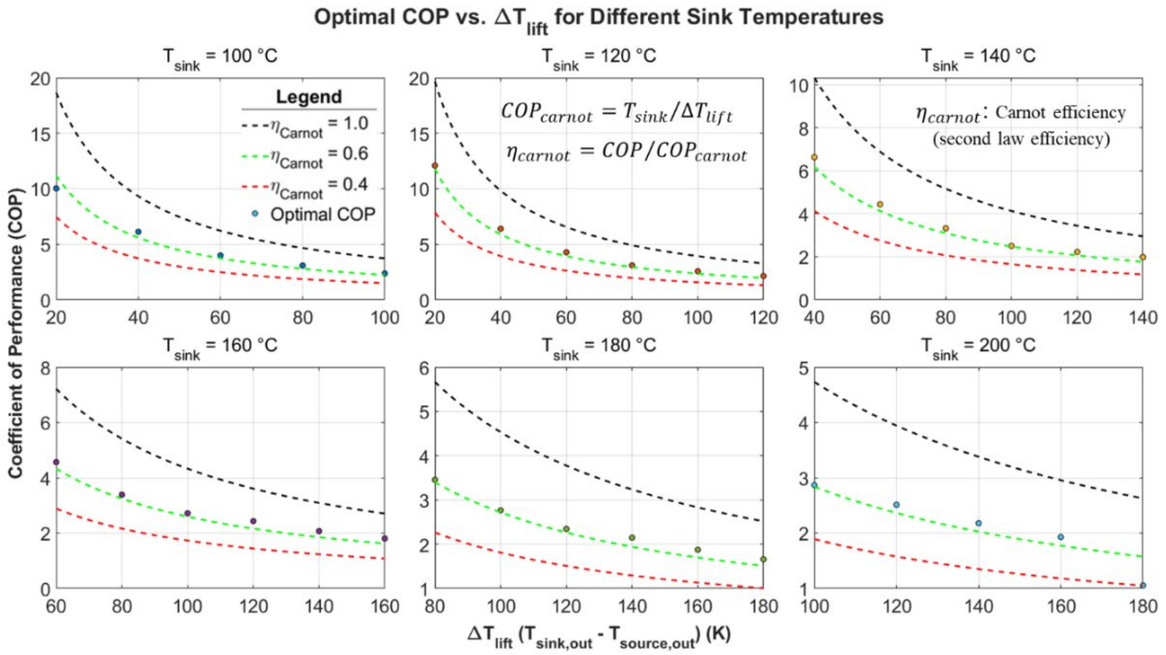

Figure 3: Optimal COP vs ΔT_{lift} for different T_{sink}

3.3. Environmental performance

The analysis revealed that TEWI was strongly correlated with ΔT_{lift}. As shown in Fig. 4, increasing ΔT_{lift} (i.e., reducing T_{source} at a given T_{sink}) increased the power input, thereby increasing the indirect impact and significantly elevating total TEWI. Notably, the optimal system at the operating condition of T_{source} = 20 °C and T_{sink} = 200 °C yielded the highest equivalent CO_2 emissions, a finding directly attributable to the system's inferior energetic performance. Analysis of the TEWI breakdown at T_{sink} = 160 °C (Fig. 5) showed that the total TEWI was almost exclusively composed of the indirect component, with direct emissions representing less than 1%, confirming the strong influence of energy consumption on the system's carbon footprint. The indirect (Scope 2) impact depended on the carbon intensity of the electricity supply, which varied with location and energy mix. In this analysis, the carbon intensity was assumed to match the average emission factor of EU fossil-fuel-based power generation. In contrast, under a fully renewable electricity scenario, this indirect impact would be negligible.

3.4. Economic performance

The economic analysis employed two metrics. The costs of the different cycles were assessed first using SPEC and then using $LCOH_{GCT}$, which provided a comprehensive evaluation by including integration, balance-of-plant (BOP), planning and installation expenses to evaluate the total CAPEX, OPEX (electricity, and O&MC for each component), as well as CO_2 emission taxes (mostly from indirect TEWI via electricity).

Since HEXs and compressors are key cost drivers in HTHP systems, particular attention was given to their cost estimation. The analysis showed that the SPEC of the optimal systems increased at low T_{source}, reaching up to 616 €/kW_{TH} for the case with T_{source}= 0 °C and T_{sink}= 180 °C, while for most conditions it remained within 200–500 €/kW_{TH}. At higher T_{source}, SPEC values converged and ΔT_{lift} had a smaller influence, except cases with T_{sink} = 200 °C. To clarify the cost structure, Fig. 6 presented the SPEC breakdown of the optimal systems at a T_{sink} of 160 °C. In most cases, compressors accounted for 60–70% of total cost, with the remaining ~30% attributed to HEXs.

The $LCOH_{GCT}$ analysis showed values between 20–100 €/MWh for all operating conditions, depending on ΔT_{lift} and T_{sink}. An exception was the optimal system at T_{source}= 20 °C and T_{sink}=200 °C, where the $LCOH_{GCT}$ increased to 133 €/MWh due to its poor energetic performance. For complete comparison, Fig. 7 presented the $LCOH_{GCT}$ breakdown of the optimal systems at a T_{sink} of 160 °C. In most cases, electricity consumption was the dominant cost, accounting for ~60%, while ~15% was associated with CO_2 emission taxes (mostly from indirect TEWI via electricity). Total CAPEX contributed ~20%.

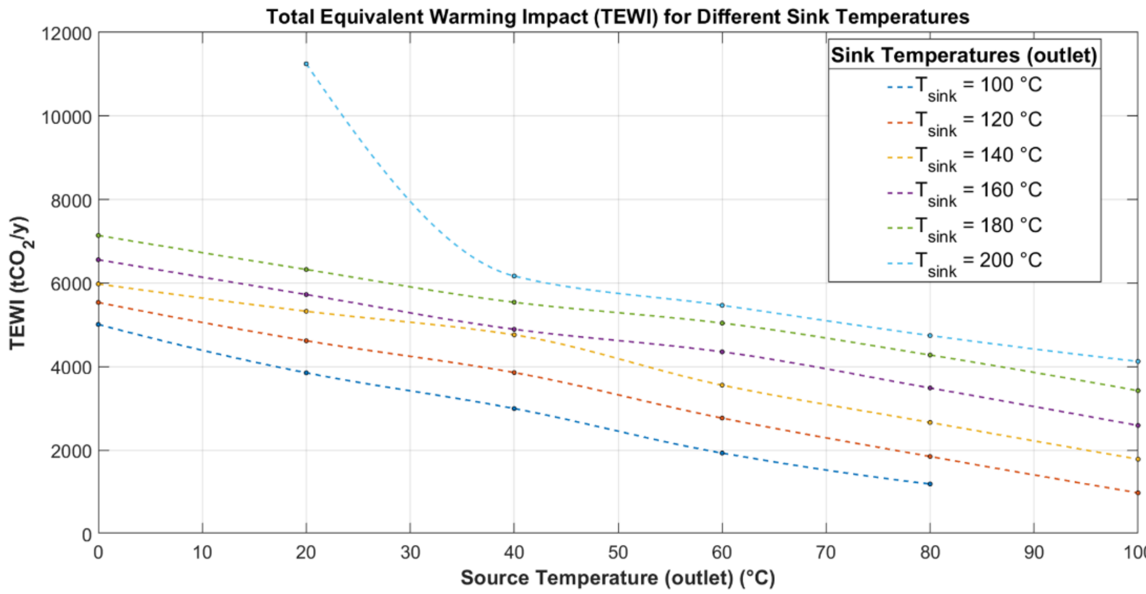

Figure 4: TEWI of the optimal cases vs T_{source} for different T_{sink} = 160 °C

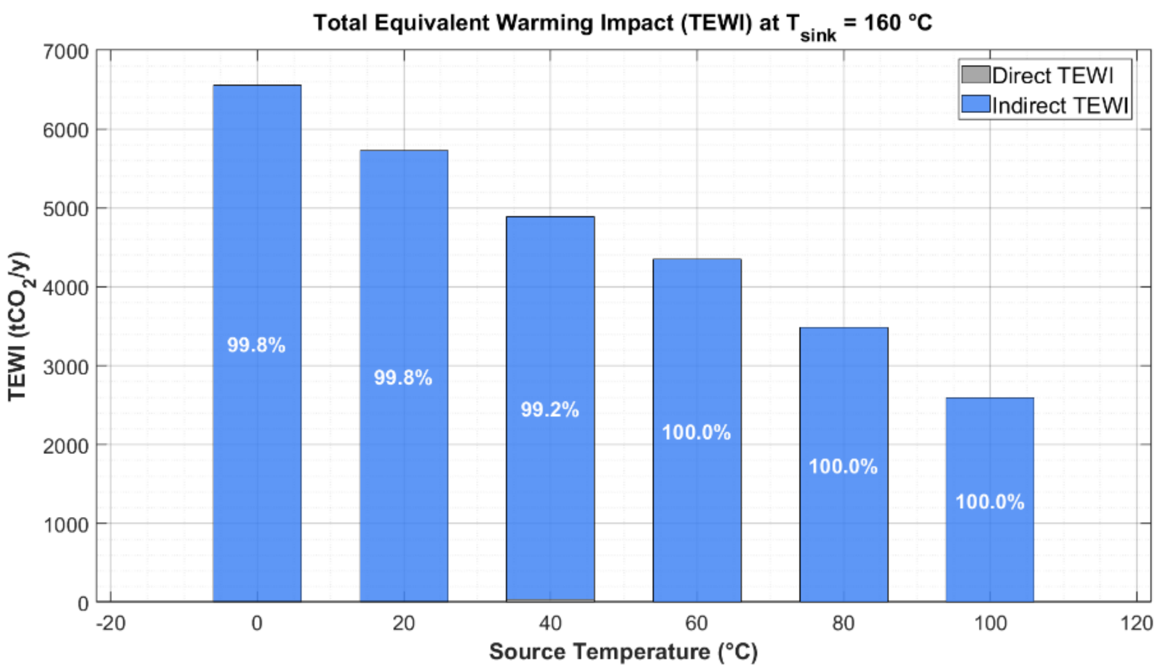

Figure 5: TEWI Breakdown of the optimal cases vs T_{source} at T_{sink} = 160 °C

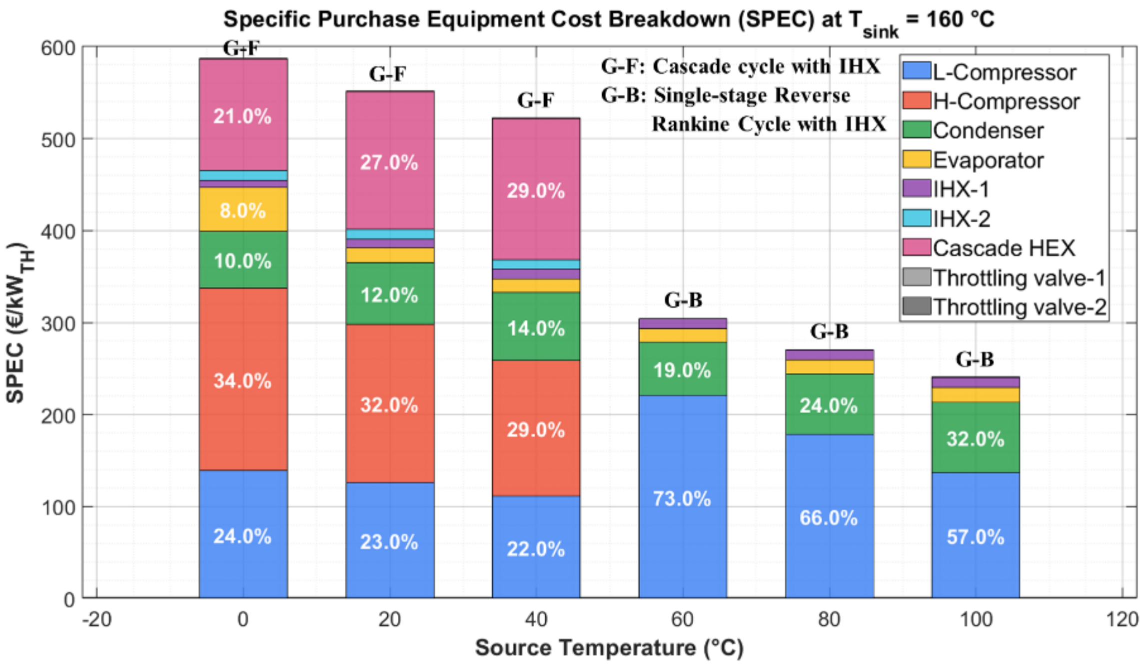

Figure 6: SPEC Breakdown of the optimal cases vs T_{source} at T_{sink} = 160 °C

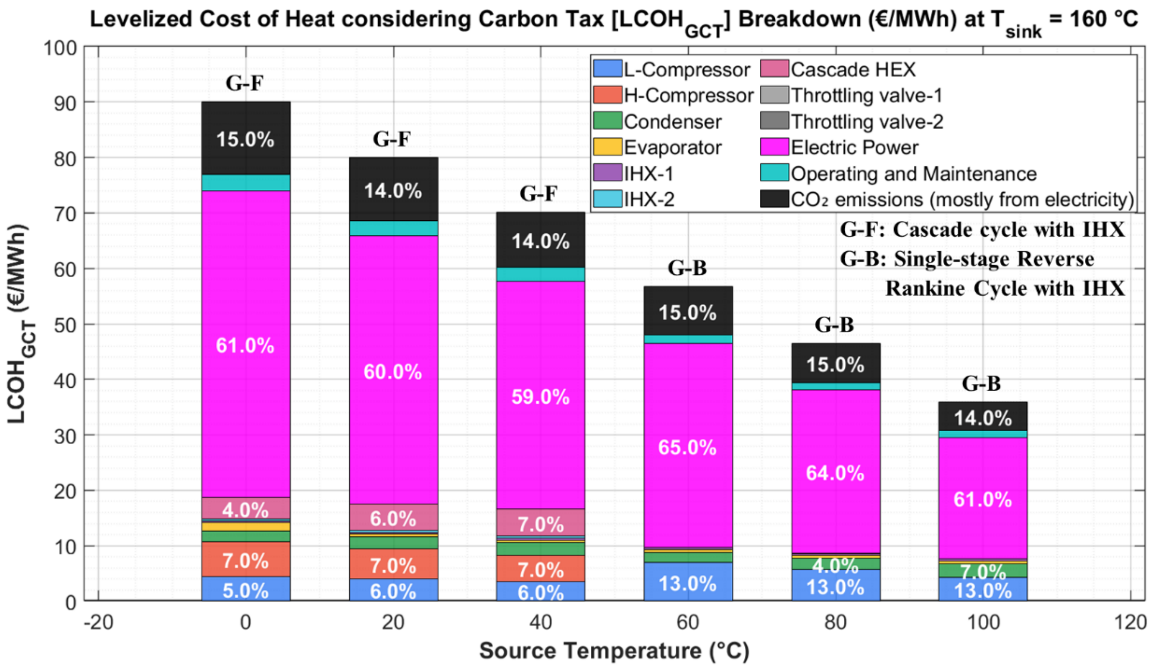

Figure 7: $LCOH_{GCT}$ Breakdown of the optimal cases vs T_{source} at T_{sink} = 160 °C

4. Conclusion

This study numerically evaluated 59 working fluids across six closed vapor compression cycles, utilizing five compressor types and two HEX technologies. The analysis simulated all possible combinations under wide operating range of high-temperature conditions, assessing them against energetic (COP, η_{carnot}), environmental (TEWI), and economic (SPEC) metrics, with $LCOH_{GCT}$ used as the primary optimization criterion. The objective was to determine the optimal HTHP design by jointly considering all these aspects for various temperature levels, thereby highlighting efficient, innovative solutions for industrial applications. The main conclusions were as follows:

- The optimal cycle configuration strongly depended on ΔT_{lift}. Single-stage cycles were optimal at low lifts (<80 K), while cascade cycles dominated at high lifts (>80 K), while two-stage flash cycles were the best option for also some intermediate cases.
- Cyclopentane, n-pentane, and methoxymethane consistently showed the highest performance, either individually in single-stage systems or paired in cascade configurations.
- Multi-stage centrifugal compressors were optimal in most cases due to the high heating capacity, which imposed large volumetric flow rates.
- Across all conditions, optimal systems converged to a η_{carnot} of ~0.6. Higher values occurred at large ΔT_{lift} with low T_{source}, conditions that reduce evaporator losses.
- Increasing ΔT_{lift} raised indirect TEWI, which dominated total impact. Direct emissions contributed <1%, confirming that system's carbon footprint is almost entirely driven by electricity consumption.
- Compressor costs dominated the SPEC, representing 60–70%, while HEXs accounted for ~30%.
- Electricity consumption (~60%) dominated the $LCOH_{GCT}$, while CO_2-emission taxes contributing ~15% and CAPEX accounting for only ~20%.

Acknowledgements

This research was supported by the project ECOSISTER funded under the National Recovery and Resilience Plan (NRRP), Mission 04 Component 2 Investment 1.5 – NextGenerationEU, Call for tender n. 3277 dated 30/12/2021, within Spoke 2 – Clean energy production, storage and saving (ECOSISTER – Ecosystem for Sustainable Transition in Emilia-Romagna). Award Number: 0001052 dated 23/06/2022

Concession Decree No. 1052 of 23/06/2022 adopted by the Italian Ministry of University and Research, CUP D93C22000460001.

References

1. de Boer R, Marina A, Zühlsdorf B, Arpagaus C, Bantle M, Wilk V, et al. Strengthening Industrial Heat Pump Innovation: Decarbonizing Industrial Heat. 2020.
2. Bamigbetan O, Eikevik TM, Nekså P, Bantle M. Review of vapour compression heat pumps for high temperature heating using natural working fluids. International Journal of Refrigeration. 2017;80:197-211.
3. Chua KJ, Chou SK, Yang WM. Advances in heat pump systems: A review. Applied Energy. 2010;87(12):3611-24.
4. Jiang J, Hu B, Wang RZ, Deng N, Cao F, Wang C-C. A review and perspective on industry high-temperature heat pumps. Renewable and Sustainable Energy Reviews. 2022;161:112106.
5. Lemmon, E.W., Bell, I.H., Huber, M.L., McLinden, M.O. NIST Standard Reference Database 23: Reference Fluid Thermodynamic and Transport Properties-REFPROP, Version 10.0, National Institute of Standards and Technology, Standard Reference Data Program, Gaithersburg, 2018. doi: https://doi.org/10.18434/T4/1502528.
6. SRM TEC, COMPRESSORS Software. Available at: https://srmtecgroup.com/products/compressors/. [Accessed Dec 16, 2024].
7. Frascold, COMPRESSORS Software. Available at: https://www.frascold.it/en/software. [Accessed Dec 16, 2024].
8. BITZER, COMPRESSORS Software. Available at: https://www.bitzer.de/us/us/tools-archive/software/software/. [Accessed Dec 16, 2024].
9. Danfoss, COMPRESSORS Software. Available at: https://www.danfoss.com/en/products/dcs/compressors/. [Accessed Dec 17, 2024].
10. Chamoun M, Rulliere R, Haberschill P, Peureux J-L. Experimental investigation of a new high temperature heat pump using water as refrigerant for industrial heat recovery. 2012.
11. Chamoun M, Rulliere R, Haberschill P, Peureux J-L. Modelica-based modeling and simulation of a twin screw compressor for heat pump applications. Applied Thermal Engineering. 2013;58(1):479-89.
12. Tian Y, Geng Y, Yuan H, Zhao Z. Investigation on water injection characteristics and its influence on the performance of twin-screw steam compressor. Energy. 2022;259:124886.
13. Zhao Z, Xing Z, Hou F, Tian Y, Jiang S. Theoretical and experimental investigation of a novel high temperature heat pump system for recovering heat from refrigeration system. Applied Thermal Engineering. 2016;107:758-67.
14. Kosmadakis G, Meramveliotakis G, Bakalis P, Neofytou P. Waste heat upgrading with high-temperature heat pumps for assisting steam generation in ships: Performance, cost and emissions benefits. Applied Thermal Engineering. 2024;236:121890.
15. Bamigbetan O, Eikevik TM, Nekså P, Bantle M, Schlemminger C. Experimental investigation of a prototype R-600 compressor for high temperature heat pump. Energy. 2019;169:730-8.
16. Navarro-Peris E, Corberán JM, Falco L, Martínez-Galván IO. New non-dimensional performance parameters for the characterization of refrigeration compressors. International Journal of Refrigeration. 2013;36(7):1951-64.
17. Zhao Z, Gao S, Tian Y, Zhang HJIJoER. Study on performance of high temperature heat pump system integrated with flash tank for waste heat recovery employed in steam production. 2021;45(14):20318-30.
18. Parra J, Cattell R, Etemad S, Pullen K, editors. Performance Measurements of a Low Specific Speed TurboClaw® Compressor. IOP Conference Series: Materials Science and Engineering; 2015: IOP Publishing.

19. Bantle M, editor Turbo-compressors: Prototype tests of mechanical vapour re-compression for steam driers. Proceedings of the 12th IEA Heat Pump Conference, Rotterdam, The Netherlands; 2017.
20. Giuffre A, Colonna P, Pini M. The Effect of Size and Working Fluid on the Multi-Objective Design of High-Speed Centrifugal Compressors. International Journal of Refrigeration. 2022;143:43-56.
21. Longo GA, Mancin S, Righetti G, Zilio C. A new model for refrigerant boiling inside Brazed Plate Heat Exchangers (BPHEs). International Journal of Heat and Mass Transfer. 2015;91:144-9.
22. Longo GA, Righetti G, Zilio C. A new computational procedure for refrigerant condensation inside herringbone-type Brazed Plate Heat Exchangers. International Journal of Heat and Mass Transfer. 2015;82:530-6.
23. Zhang C, Liu C, Wang S, Xu X, Li Q. Thermo-economic comparison of subcritical organic Rankine cycle based on different heat exchanger configurations. Energy. 2017;123:728-41.
24. Dalkilic AS, Acikgoz O, Tapan S, Wongwises S. Fundamental basis and implementation of shell and tube heat exchanger project design: condenser and evaporator study. Heat and Mass Transfer. 2016;52(12):2863-78.
25. Arpagaus C, Bless F, Bertsch S, Krummenacher P, Flórez-Orrego DA, Pina EA, et al., editors. Integration of high-temperature heat pumps in Swiss industrial processes (HTHP-CH). 14th IEA heat pump conference; 2023.
26. Ommen T, Jensen JK, Markussen WB, Reinholdt L, Elmegaard B. Technical and economic working domains of industrial heat pumps: Part 1 – Single stage vapour compression heat pumps. International Journal of Refrigeration. 2015;55:168-82.
27. Shamoushaki M, Niknam PH, Talluri L, Manfrida G, Fiaschi D. Development of Cost Correlations for the Economic Assessment of Power Plant Equipment. 2021;14(9):2665.
28. Hosseinnia SM, Poncet S, Nesreddine H, Monney D. Technical-economic-environmental analysis of high temperature cascade heat pump with R718 (high stage) and six different low global warming potential refrigerants (low stage). Energy Conversion and Management. 2023;292:117356.
29. Mosaffa AH, Farshi LG, Infante Ferreira CA, Rosen MA. Exergoeconomic and environmental analyses of CO2/NH3 cascade refrigeration systems equipped with different types of flash tank intercoolers. Energy Conversion and Management. 2016;117:442-53.
30. eurelectric, Wholesale Electricity Price, EU annual day-ahead Price. Available at: https://electricity-data.eurelectric.org/electricity-price.html. [Accessed Mar 12, 2025].
31. Makhnatch P, Khodabandeh R. The Role of Environmental Metrics (GWP, TEWI, LCCP) in the Selection Of Low GWP Refrigerant. Energy Procedia. 2014;61:2460-3.
32. Mateu-Royo C, Arpagaus C, Mota-Babiloni A, Navarro-Esbrí J, Bertsch SS. Advanced high temperature heat pump configurations using low GWP refrigerants for industrial waste heat recovery: A comprehensive study. Energy Conversion and Management. 2021;229:113752.
33. TRADING ECONOMICS, EU Carbon Permits, carbon emissions tax prices. Available at: https://tradingeconomics.com/commodity/carbon. [Accessed Jan 17, 2025].
34. Hamada MA, Gatti M, Molinaroli L. A Numerical Framework for Optimizing Working Fluid selection and Cycle Configurations in High-Temperature Heat Pumps for Industrial Applications: Methodology and a Case Study. Journal of Physics: Conference Series. 2025;3143(1):012108.